



CHORUS

This is the accepted manuscript made available via CHORUS. The article has been published as:

Band alignment and p-type doping of ZnSnN₂

Tianshi Wang, Chaoying Ni, and Anderson Janotti

Phys. Rev. B **95**, 205205 — Published 31 May 2017

DOI: [10.1103/PhysRevB.95.205205](https://doi.org/10.1103/PhysRevB.95.205205)

Band alignment and p -type doping of ZnSnN_2

Tianshi Wang, Chaoying Ni, Anderson Janotti

Department of Materials Science and Engineering,

University of Delaware, Newark, DE 19716.

(Dated: May 3, 2017)

Abstract

Composed of earth abundant elements, ZnSnN_2 is a promising semiconductor for photovoltaic and photoelectrochemical applications. However, basic properties such as the precise value of the band gap and the band alignment to other semiconductors are still unresolved. For instance, reported values for the band gap vary from 1.4 to 2.0 eV. In addition, doping in ZnSnN_2 remains largely unexplored. Using density functional theory with the Heyd-Scuseria-Ernzerhof hybrid functional (HSE), we investigate the electronic structure of ZnSnN_2 , its band alignment to GaN and ZnO, and the possibility of p -type doping. We find that the position of the valence-band maximum (VBM) of ZnSnN_2 is 0.39 eV higher than that in GaN, yet the conduction-band minimum (CBM) is close to that in ZnO, which suggests that achieving p -type conductivity is likely as in GaN, yet it may be difficult to control unintentional n -type conductivity as in ZnO. Among possible p -type dopants, we explore Li, Na, and K substituting on the Zn site. We show that while Li_{Zn} is a shallow acceptor, Na_{Zn} and K_{Zn} are deep acceptors, which we trace back to large local relaxations around the Na and K impurities due to the atomic size mismatches.

6 I. INTRODUCTION

7 The nitrides Zn-IV-N₂ are promising semiconductor materials for photovoltaic and pho-
8 toelectrochemical cells,¹ and could also complement the group-III nitrides and their alloys
9 in optoelectronic and electronic applications.² By adding Si and Ge, the direct band gap of
10 Zn(Si,Ge,Sn)N₂ alloys are predicted to cover all the visible-light spectrum,³⁻⁵ making them
11 promising for full-spectrum LED applications. In contrast, InGaN alloys can be hardly used
12 at longer wavelengths beyond the blue and green spectral regions, in part due to segregation
13 at high indium concentrations.⁶⁻⁸ In addition, in Zn-IV-N₂, Zn, Si and Sn are earth abundant
14 and environment friendly as opposed to the increasingly high cost of indium. The crystal
15 structure of Zn-IV-N₂ is derived from that of wurtzite III-nitride, where the group-III ions
16 are replaced by alternating Zn and group-IV ions, resulting in an orthorhombic structure as
17 shown in Fig. 1(a). The local valence requirement of two electrons per bond is still fulfilled.
18 ZnSnN₂ is an example of this class of ternary nitrides. It has been synthesized by different
19 methods, including vapor-liquid-solid method,³ reactive radio frequency magnetron sputter-
20 ing deposition,⁹ and molecular beam epitaxy (MBE);¹⁰ nevertheless, ZnSnN₂ is still at early
21 stages of development.⁵

22 The calculated band gap of ZnSnN₂ is direct at Γ , yet the reported values vary in a wide
23 range, from 1.4 eV to 2.0 eV.^{2,5,9,11,12} Calculations based on the Heyd-Scuseria-Ernzerhof
24 (HSE) hybrid functional give a gap of 1.42 eV for mixing parameter $\alpha=0.25$ (25% Hartree-
25 Fock exchange)⁹ and 1.84 eV for $\alpha=0.31$,^{2,13} while calculations based on the PBE0 hybrid
26 functional give a gap of 2 eV.¹² Using the quasiparticle self-consistent GW method *Punya*
27 *et al.*⁴ reported a gap of 2.15 eV using lattice parameters based on the local density approx-
28 imation (LDA) and, more recently, 1.8 ± 0.1 eV¹¹ using experimental values for the lattice
29 parameters. Experimental values for the band gap, based on the absorption onset or photo-
30 luminescence spectra, lie in a wider range, from 0.95 to 2.38 eV.^{3,9,14-17} It has been argued
31 that ZnSnN₂ samples are typically *n*-type with high free carrier concentrations in the range
32 10^{18} - 10^{21} cm⁻³,^{9,14} leading to a significant Burstein-Moss shift that explains the observed
33 larger band gap values,⁹ while lower band gap values are attributed to high degrees of cation
34 disorder.^{5,14} Recent experiments indicate that a wurtzite phase can be also stabilized at low
35 growth temperatures,¹⁸ and this could also possibly explain the observed lower band gaps.

36 Based on results of first-principles calculations, *Chen et al.*¹³ explained that ZnSnN₂

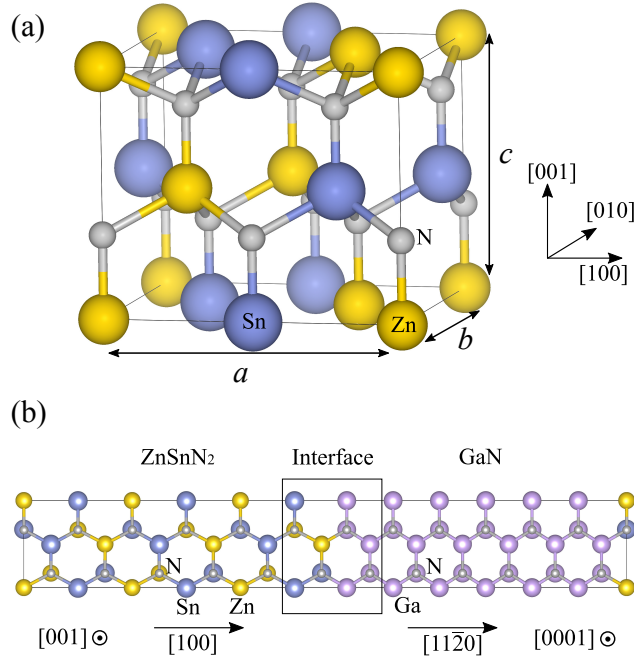


FIG. 1. (Color online) (a) ZnSnN_2 $Pna2_1$ orthorhombic structure. The lattice parameters a , b , and c are indicated. (b) Structure of the $\text{ZnSnN}_2/\text{GaN}$ (ZnO) superlattice used for determining the alignment of the averaged electrostatic potential in the bulk regions of ZnSnN_2 and GaN (ZnO).

37 is n -type because of low formation energy of native defects that act as shallow donors,
 38 such as Sn_{Zn} antisites, and possible contamination by O_{N} impurities. Recent experiments
 39 corroborate this picture by finding that the carrier density can be tuned by changing the
 40 cation composition ratio.¹⁷ As yet, p -type doping has not been explored. It is not clear if
 41 ZnSnN_2 could be made p -type as GaN , or whether p -type conductivity would be difficult
 42 to realize as in ZnO . *Punya et al.*¹¹ calculated band offsets between ZnSnN_2 , GaN and
 43 ZnO using the quasiparticle self-consistent GW method. They reported that the VBM of
 44 ZnSnN_2 is higher than that of GaN by 1.9 eV.¹¹ This very large valence-band offset is difficult
 45 to explain because it represents a huge and unexpected deviation from the common anion
 46 rule.¹⁹ For furthering the development of ZnSnN_2 as a semiconductor for device applications,
 47 it is essential to know a series of basic properties besides the band gap, e.g., the position of
 48 the band edges with respect to that of other semiconductors, and how to control electrical
 49 conductivity— is it possible to achieve both n -type and p -type conductivity in ZnSnN_2 ?

50 Here we use density functional calculations based on the HSE hybrid functional to de-

51 termine the electronic band structure of ZnSnN_2 and the band offsets between ZnSnN_2 and
52 two common wide-band-gap semiconductors, wurtzite GaN and ZnO. We also explore the
53 possibility of p -type doping in ZnSnN_2 . In the following, we first describe the details of the
54 calculations, and present the results for the electronic band structure; then we discuss the
55 results for the band alignment, and finally we address p -type doping, exploring alkali metals
56 Li, Na, and K substituting on the Zn site as possible shallow acceptors.

57 II. COMPUTATIONAL METHODS

58 Our calculations are based on the density functional theory (DFT)^{20,21} and the screened
59 hybrid functional of Heyd-Scuseria-Ernzerhof (HSE)²² as implemented in the VASP code.^{23,24}
60 In the HSE approach, the exchange potential is separated into short-range and long-range
61 parts, and the non-local Hartree-Fock exchange is mixed with the generalized gradient ap-
62 proximation (GGA) exchange²⁵ only in the short-range part. The fraction of Hartree-Fock
63 exchange is represented by a mixing parameter α , with a typical value of 0.25. The HSE
64 functional has been shown to produce accurate band gaps for many semiconductors,^{26,27} in
65 contrast to the LDA or the GGA which severely underestimate band gaps.²⁸ However, in the
66 case of GaN and ZnO, α must be increased to 0.31 and 0.38 for a correct description of band
67 gaps, band alignments, and defect levels.²⁹⁻³¹ A test using the GW within the G_0W_0 ap-
68 proximation, as implemented in the VASP code, on top of the HSE calculation with $\alpha=0.25$
69 gives a correction of only 0.1 eV to the quasiparticle band gap compared to that of HSE
70 with $\alpha=0.31$. Therefore, we use HSE with $\alpha=0.31$, as in GaN, for the band structure and
71 impurity calculations in ZnSnN_2 .

72 Projector augmented wave (PAW) potentials are used to describe the interaction between
73 the valence electrons and the frozen ion cores.³² The PAW potentials for Zn, Sn, and N
74 contain 12, 4, and 5 valence electrons, respectively, i.e., Zn: $3d^{10}4s^2$, Sn: $5s^25p^2$, N: $2s^23p^3$.
75 For obtaining the equilibrium lattice parameters of ZnSnN_2 , we used the orthorhombic cell
76 with 16 atoms shown in Fig. 1(a), with a $4\times 4\times 4$ mesh of k -points for integrations over the
77 Brillouin zone. For GaN and ZnO, we used the primitive wurtzite cell with 4 atoms, with
78 $6\times 6\times 4$ mesh of k -points. We use a cutoff of 500 eV for the plane wave basis set in all
79 calculations.

The formation enthalpy of ZnSnN₂ is given by:

$$\begin{aligned} \Delta H^f(\text{ZnSnN}_2) = & E_{tot}(\text{ZnSnN}_2) - E_{tot}(\text{Zn}) \\ & - E_{tot}(\text{Sn}) - E_{tot}(\text{N}_2), \end{aligned} \quad (1)$$

80 where $E_{tot}(\text{ZnSnN}_2)$ is the total energy per formula unit of ZnSnN₂, $E_{tot}(\text{Zn})$ and $E_{tot}(\text{Sn})$
 81 are the total energies of bulk Zn in hexagonal-close-packed structure and Sn in the diamond
 82 crystal structure. The last term, $E_{tot}(\text{N}_2)$, is the total energy of an isolated N₂ molecule.

83 The band alignment between ZnSnN₂ and GaN (ZnO) is calculated using a standard
 84 procedure as described elsewhere.³³ First, the VBM of ZnSnN₂ and GaN (ZnO) are deter-
 85 mined with respect to the averaged electrostatic potential in bulk calculations. Then, the
 86 averaged electrostatic potentials are aligned by performing an interface calculation. In this
 87 case, we used a supercell comprised of 12 layers of each material with two equivalent inter-
 88 faces, in a superlattice configuration as shown in Fig. 1(b). We chose a superlattice along
 89 the non-polar [100] direction of the ZnSnN₂ orthorhombic structure and $[11\bar{2}0]$ of the GaN
 90 (ZnO) wurtzite crystal structure to avoid the directions of spontaneous polarization, and
 91 the problems resulting from the polar discontinuity. The positions of the atoms in the bulk
 92 regions of the superlattice were fixed and the positions of the atoms at the interface layers
 93 were allowed to relax. The in-plane lattice parameters were set to the average of those of
 94 ZnSnN₂ and GaN (ZnO) and the out-of-plane dimensions were chosen such that the equi-
 95 librium volume of each material is conserved. We also have tested using the in-plane lattice
 96 parameters of GaN and of ZnSnN₂, making sure that the volume of the strained material
 97 is equal to its equilibrium volume. The results of these tests show an error of ± 0.07 eV
 98 in the averaged electrostatic potential differences. For the mixing parameter in HSE, we
 99 tested using $\alpha = 0.25, 0.31,$ and 0.38 for the superlattice calculations. We find the averaged
 100 electrostatic potential differences for the three mixing parameters vary within 0.05 eV. This
 101 is expected since the averaged electrostatic potential contains only the Hartree term, and
 102 depends mostly on the volume as long as the PAW potentials and the number of electrons
 103 are kept the same.

104 The calculations described above are for natural band offsets, i.e., the relative position
 105 of the band edges of two materials, in their equilibrium structures, with respect to the
 106 vacuum level. We have also considered a pseudomorphic interface where the in-plane lattice
 107 parameters are those of GaN and the out-of-plane lattice parameter of the heterostructure

108 is allowed to relax, minimizing the total energy. Since the ZnSnN₂ layer is compressed in
 109 the in-plane directions, it expands in the out-of-plane direction but does not fully recover
 110 its equilibrium volume. This is referred to strained ZnSnN₂ case below. By comparing the
 111 natural band offset with the band offset for GaN/ZnSnN₂ with strained ZnSnN₂, we derive
 112 absolute deformation potentials for the valence band (a_v) and for the conduction band (a_c),
 113 and compare to the reported values for GaN and ZnO.³³

The calculations for impurities in ZnSnN₂ are carried out using a supercell of 128 atoms,
 which is a 2×2×2 repetition of the 16-atom unit cell, with $(\frac{1}{4}, \frac{1}{4}, \frac{1}{4})$ as special k -point for
 integrations over the Brillouin zone. As acceptor impurities, we considered Li, Na, and K
 substituting on the Zn site, in analogy to Mg doping in GaN. The likelihood of incorporating
 an impurity in a crystal is determined by its formation energy. In this case, the formation
 energy of a defect (e.g., Li_{Zn}) in charge state q is defined as:³¹

$$E^f(\text{Li}_{\text{Zn}}^q) = E_{\text{tot}}(\text{Li}_{\text{Zn}}^q) - E_{\text{tot}}(\text{ZnSnN}_2) + E_{\text{tot}}(\text{Zn}) + \mu_{\text{Zn}} \\ - E_{\text{tot}}(\text{Li}) - \mu_{\text{Li}} + q(\varepsilon_F + E_v) + \Delta^q, \quad (2)$$

114 where $E_{\text{tot}}(\text{Li}_{\text{Zn}}^q)$ is the total energy of the supercell containing one Li sitting on a Zn site in
 115 charge state q , and $E_{\text{tot}}(\text{ZnSnN}_2)$ is the total energy of a perfect ZnSnN₂ crystal in the same
 116 supercell. The chemical potential of Li (μ_{Li}) is referenced to the total energy per atom of Li
 117 bulk [$E_{\text{tot}}(\text{Li})$], whereas μ_{Zn} is referenced to the total energy per atom of Zn bulk [$E_{\text{tot}}(\text{Zn})$].
 118 The energy of the electron reservoir is the Fermi level ε_F , referenced to the valence-band
 119 maximum E_v of bulk ZnSnN₂. Finally, Δ^q is the correction due to the finite size of the
 120 supercell.³⁴

121 III. RESULTS AND DISCUSSION

122 A. Crystal structure and electronic structure

123 The calculated lattice parameters of ZnSnN₂, GaN, and ZnO are listed in Table I. The
 124 results are in good agreement with previous calculations^{13,30,35} and experimental data.^{3,36,37}
 125 The calculated formation enthalpy of ZnSnN₂ is −0.23 eV, in agreement with the value
 126 of −0.17 eV from previous calculations.¹³ The small formation enthalpy indicates that the
 127 synthesis of high quality ZnSnN₂ using the stable phase of the composing elements can be
 128 quite challenging.⁵

TABLE I. Calculated equilibrium lattice parameters for ZnSnN₂, GaN and ZnO using the HSE hybrid functional with mixing parameters $\alpha = 0$ (GGA), 0.25, 0.31, and 0.38. For comparison, the experimental values are also listed: for GaN from Ref. 36, for ZnO from Ref. 37, and for ZnSnN₂ from Ref. 3.

		GGA	$\alpha = 0.25$	$\alpha = 0.31$	$\alpha = 0.38$	Exp.
GaN	a (Å)	3.247	3.201	3.192	3.181	3.19
	c (Å)	5.281	5.202	5.185	5.167	5.19
ZnO	a (Å)	3.282	3.261	3.255	3.249	3.248
	c (Å)	5.319	5.232	5.218	5.203	5.204
ZnSnN ₂	a (Å)	6.810	6.743	6.733	6.712	6.753
	b (Å)	5.912	5.855	5.839	5.827	5.842
	c (Å)	5.543	5.468	5.452	5.436	5.462

129 The electronic band structure of ZnSnN₂ is shown in Fig. 2(a). ZnSnN₂ has a direct band
130 gap at the Γ point. The calculated band gap using the HSE functional depends on the mixing
131 parameter α . For $\alpha = 0.31$, we obtain a gap of 1.75 eV, in good agreement with previous
132 calculations.¹³ Room-temperature photoluminescence excitation spectroscopy measurements
133 give a value of 1.7 ± 0.1 eV.³ For comparison, GGA ($\alpha = 0$) severely underestimates the
134 band gap, resulting in a gap of only 0.1 eV. Compared to the GGA value with the lattice
135 parameters fixed to those obtained using HSE with $\alpha = 0.31$, we find that HSE corrects the
136 gap by pushing down the valence band by 0.60 eV and pushing up the conduction band by
137 0.90 eV. As shown in the electronic band structure of ZnSnN₂ [Fig. 2(a)], the relatively flat
138 Zn 3*d* bands show up at ~ 7 eV below the VBM. The CBM, on the other hand, is derived
139 mostly from Zn *s* orbitals.

140 B. Band alignments

141 The calculated band alignment between ZnSnN₂ and GaN and between ZnSnN₂ and ZnO
142 are shown in Fig. 2(b). For these calculations, we used lattice parameters obtained in HSE
143 using $\alpha = 0.31$ for ZnSnN₂ and GaN, and $\alpha = 0.38$ for ZnO. The VBM with respect to the
144 averaged electrostatic in the bulk calculations was determined using $\alpha=0.25$ and 0.31 for

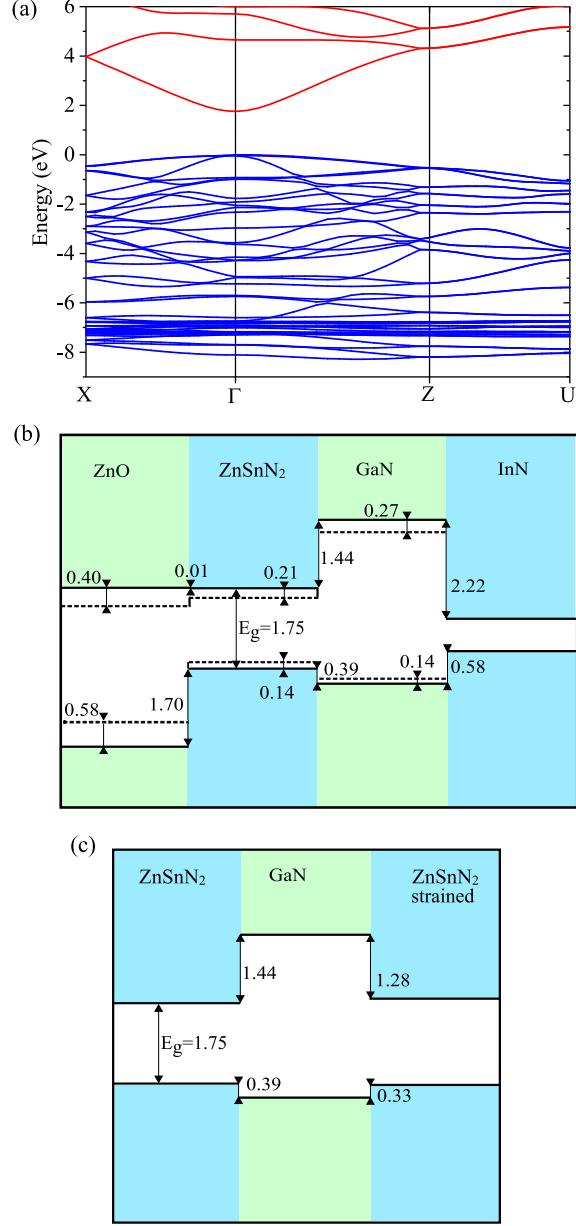


FIG. 2. (Color online)(a) Calculated electronic band structure of ZnSnN₂ using HSE with mixing parameter $\alpha = 0.31$. The zero in the energy axis correspond to the valence-band maximum. (b) Band alignment between ZnSnN₂ and GaN, and between ZnSnN₂ and ZnO. These correspond to natural band offsets, i.e. the relative position of the band edges in each material, in their equilibrium lattice parameters. The experimental value for the band alignment between GaN and InN, from Ref. 38, is also included. The dashed lines correspond to results using mixing parameter $\alpha = 0.25$ in HSE. (c) Band alignment at the GaN/ZnSnN₂ for unstrained and strained (pseudomorphic) ZnSnN₂ cases. All values are in eV.

145 ZnSnN₂ and GaN, and $\alpha = 0.25$ and 0.38 for ZnO. Again, we note that the difference in the
146 averaged electrostatic potentials in the interface calculations does not depend on the mixing
147 parameter, as long as the volume of the superlattice is kept fixed.

148 We find that the VBM of ZnSnN₂ is higher than that of GaN by 0.39 eV. This can be
149 attributed largely to the stronger repulsion between the Zn $3d$ states and the N $2p$ states in
150 ZnSnN₂ than that between the Ga $3d$ and N $2p$ in GaN. Note that this result is independent
151 of the mixing parameter α . We also find that the VBM of ZnSnN₂ is 1.70 eV higher than
152 that of ZnO, and this is attributed largely to the difference in the energetic position of the N
153 $2p$ and O $2p$ orbitals. These results are in contrast to those in Ref. 11 where a valence-band
154 offset of 1.9 eV is reported for ZnSnN₂ and GaN. Based on the common anion rule, one
155 would expect the valence band offset between ZnSnN₂ and GaN to be much smaller, as our
156 results indicate. Moreover, based on the transitivity rule, we obtain a valence band offset
157 between GaN and ZnO of 1.31 eV, in good agreement with the value of 1.37 eV deduced from
158 measurements of x-ray photoemission spectroscopy for ZnO/AlN and established values for
159 GaN/AlN.³⁹ We note, however, that our results are in disagreement with the experimental
160 results of Liu *et al.*⁴⁰ which reported values between 0.7 and 0.9 eV for the valence band
161 offset at the GaN/ZnO interface, and these are close to those predicted by Punya *et al.*¹¹
162 and Huda *et al.*,⁴¹ the latter using DFT+ U . In the case of the conduction-band offset, we
163 find that the CBM of ZnSnN₂ is 1.44 eV lower than that of GaN. In ZnSnN₂, the lowest
164 conduction band is derived from Zn $4s$ states which is much lower in energy than that in
165 GaN, derived from Ga $4s$ states. Based on a similar argument, we find that the CBM of
166 ZnSnN₂ is only 0.01 eV lower than that in ZnO, since in both materials the lowest energy
167 conduction band is derived mostly from the Zn $4s$ states. In all, further experiments are
168 called for solving the discrepancies in the calculated band alignments.

169 For the band offset between GaN and the pseudomorphic ZnSnN₂ layer, where the in-
170 plane lattice parameters are those of GaN and the out-of-plane lattice parameter of the
171 heterostructure is allowed to relax, we find a valence-band offset of 0.33 eV and a conduction-
172 band offset of 1.28 eV. The volume of the strained ZnSnN₂ is 5.64% smaller than the equi-
173 librium volume. From the calculations of the band alignments between GaN and unstrained
174 ZnSnN₂ and between GaN and strained (pseudomorphic) ZnSnN₂ shown in Fig. 2(c), we de-
175 termined the absolute deformation potential for the valence band a_v and for the conduction
176 band a_c . We find $a_v=1.06$ eV and $a_c=-2.84$ eV; for the band gap deformation potential we

177 find $a_g = -3.90$ eV. These results are within the range of values reported for GaN and ZnO,³³
178 since the valence-band maximum of ZnSnN₂ is derived from N 2*p* and the conduction-band
179 minimum is derived from Zn 4*s* states.

180 Based on the calculated position of the band edges of ZnSnN₂ with respect to those of
181 GaN and ZnO we can infer on the possibility of *n*-type and *p*-type doping. For instance,
182 ZnO can be made *n*-type quite easily, largely due to the low position of its CBM in an
183 absolute energy scale.⁴² Most donor impurities, including H,⁴³ result in shallow donor levels.
184 We therefore expect the same conclusions to hold in the case of ZnSnN₂. On the other hand,
185 ZnO cannot be made *p*-type by substituting Li or Na on the Zn site, since these impurities
186 are deep acceptors. This can be attributed to the VBM in ZnO being too low with respect
187 to the vacuum level.⁴⁴ All the acceptor impurities tested so far seem to lead to deep acceptor
188 levels.⁴² On the other hand, GaN can be made *p*-type by incorporating Mg on the Ga site.
189 Since the VBM of ZnSnN₂ is higher than that of GaN by 0.39 eV, one would expect that
190 ZnSnN₂ could be made *p*-type as GaN. Similar arguments can be used in comparison with
191 InN, which has been shown to be *p*-type dopable. However, its low lying conduction band
192 poses difficulties in reducing unintentional *n*-type conductivity.⁴⁵

193 C. Acceptor impurities in ZnSnN₂

194 For achieving *p*-type doping in ZnSnN₂, one would need an impurity with one less valence
195 electron than one of the host atoms. For example, C substituting on the N site. However,
196 C is a deep acceptor in GaN with the acceptor level at 0.9 eV above the VBM,⁴⁶ and it is
197 likely to behave as deep acceptor in ZnSnN₂ as well. Besides, C could prefer to replace Sn
198 and be electrically inactive. Choosing a column-III element to substitute on the Sn site can
199 be problematic as well, since these impurities could also replace Zn and act as donors. Here,
200 as candidates for shallow acceptors in ZnSnN₂, we considered Li, Na, and K substituting on
201 the Zn site. Although Li, Na, and K could also incorporate at interstitial sites and behave
202 as donors, we expect these interstitial species to be highly mobile and, therefore, be easily
203 removed in post-growth annealing. Analogous strategy has been recently demonstrated by
204 recent experiments on Zn-rich annealed ZnSnN₂ with added hydrogen.⁴⁷ The results reveal
205 that post-growth annealing removes hydrogen and reduces carrier density down to 4×10^{16}
206 cm⁻³, suggesting that H were passivating acceptors.

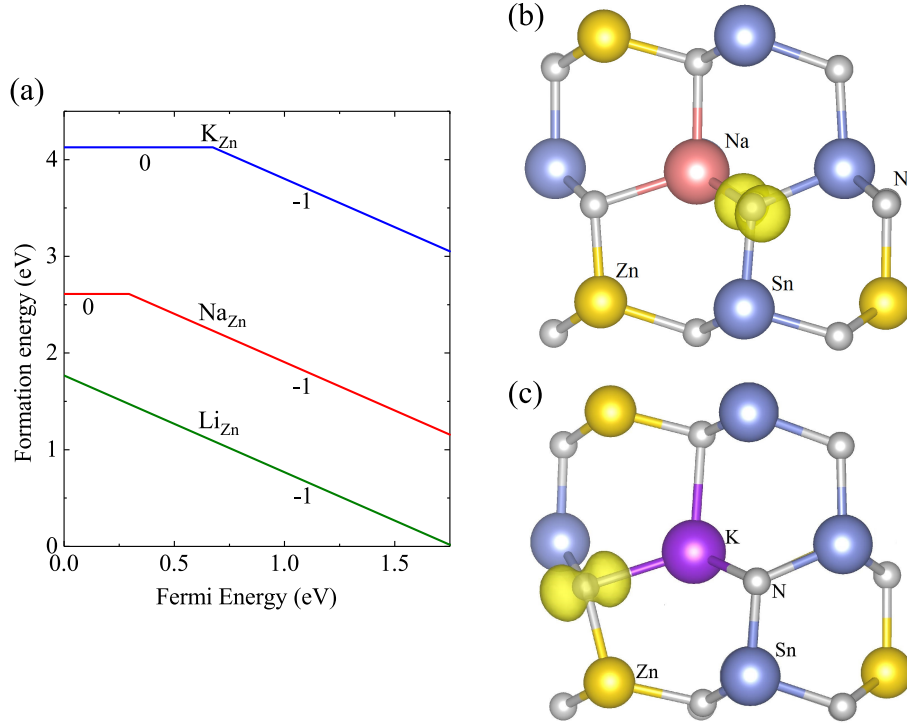


FIG. 3. (Color online) (a) Formation energy of Li, Na, and K impurities in two charge states 0 and -1 as function of the Fermi level. (b) and (c) Calculated spin density of charge neutral Na_{Zn} and K_{Zn} in $ZnSnN_2$. The isosurface is 10% of the maximum density.

207 The formation energy of Li_{Zn} , Na_{Zn} , and K_{Zn} in $ZnSnN_2$ are shown in Fig. 3(a). We find
 208 that Li displays shallow acceptor behavior, with the hole being delocalized over the whole
 209 supercell. Therefore, we only plot the formation energy of Li_{Zn} in the negative charge state.
 210 On the other hand, we find Na_{Zn} and K_{Zn} to behave as a deep acceptors, with (0/-) acceptor
 211 levels at 0.30 eV and 0.68 eV above the VBM. Since the formation enthalpy of $ZnSnN_2$ is
 212 rather small (-0.23 eV), we only plotted the formation energies for Zn-rich condition.

213 The formation energies calculated with respect to the elemental phases of Li, Na, and K
 214 show an interesting trend. It monotonically increases from Li, Na, to K. We attribute this
 215 behavior to the size mismatch between the impurity and the host Zn atom. While Li_{Zn} only
 216 slightly affects the lattice by causing small displacements of the nearest neighbor N atoms,
 217 by 0.5% of the equilibrium bond length, Na_{Zn} and K_{Zn} cause rather large displacements, of
 218 8.5% (Na_{Zn}) and 16.2% (K_{Zn}) of the nearest neighbor N atoms. The displacements caused
 219 by K_{Zn} are so large that makes the neighboring N assume almost planar configurations.

220 The local lattice relaxations and the charge density distribution of the hole associated
221 with neutral Na_{Zn} and K_{Zn} in ZnSnN_2 are shown in Fig. 3(b) and (c). The hole from charge
222 neutral Na_{Zn} or K_{Zn} becomes localized on one of the neighboring N, and in the case of
223 K_{Zn} the N-K distance is 2.40 Å, compared to 2.07 Å for the equilibrium Zn-N bond length.
224 Therefore, we conclude that, only Li_{Zn} effectively acts as shallow acceptor in ZnSnN_2 , in
225 part due to the small perturbation of the local lattice structure. However, we note that as
226 in InN, it may be difficult to reduce the unintentional n -type conductivity in ZnSnN_2 due
227 to the low lying conducting band.

228 IV. SUMMARY

229 In conclusion, we performed hybrid functional calculations for ZnSnN_2 to determine its
230 band gap and band alignment to GaN and ZnO, and to explore the possibility of p -type
231 doping. We find that ZnSnN_2 has a band gap of 1.75 eV, in agreement with previous
232 calculations and experiments. The VBM of ZnSnN_2 is predicted to be 0.39 eV higher than
233 that of GaN and 1.70 eV higher than that of ZnO. The CBM of ZnSnN_2 , on the other hand,
234 is only 0.01 eV lower than that of ZnO. These results indicate that ZnSnN_2 can be made
235 p -type as GaN, and that controlling the unintentional n -type conductivity can be difficult
236 as in ZnO. For achieving p -type conductivity, we find that Li substituting on the Zn site
237 displays shallow acceptor behavior, whereas Na and K leads to deep levels. The deep level
238 behavior of Na_{Zn} and K_{Zn} are attributed to very large lattice relaxations that make the
239 neighboring N atoms assume almost planar positions with the hole localized on one of them.

240 V. ACKNOWLEDGMENTS

241 TW and CN gratefully acknowledge financial support from the II-VI Foundation, and AJ
242 thanks for the financial support from National Science Foundation under Grant No. 1652994.
243 This research was supported through the use of the Extreme Science and Engineering Dis-
244 covery Environment (XSEDE) supercomputer facility, National Science Foundation grant
245 number ACI-1053575, and the Information Technologies (IT) resources at the University of

246 Delaware, specifically the high-performance computing resources.

- 247 ¹ A. Zakutayev, *J. Mater. Chem. A* **4**, 6742 (2016).
- 248 ² P. Narang, S. Chen, N. C. Coronel, S. Gul, J. Yano, L. W. Wang, N. S. Lewis, and H. A.
249 Atwater, *Adv. Mater.* **26**, 1235 (2014).
- 250 ³ P. C. Quayle, K. He, J. Shan, and K. Kash, *MRS Commun.* **3**, 135 (2013).
- 251 ⁴ A. Punya, W. R. L. Lambrecht, and M. Van Schilfgaarde, *Phys. Rev. B* **84**, 165204 (2011).
- 252 ⁵ T. D. Veal, N. Feldberg, N. F. Quackenbush, W. M. Linhart, D. O. Scanlon, L. F. J. Piper,
253 and S. M. Durbin, *Adv. Energy Mater.* **5**, 1501462 (2015).
- 254 ⁶ Z. Liliental-Weber, D. N. Zakharov, K. M. Yu, J. W. Ager III, W. Walukiewicz, E. E. Haller,
255 H. Lu, and W. J. Schaff, *J. Electron Microsc.* **54**, 243 (2005).
- 256 ⁷ M. K. Horton, S. Rhode, S. L. Sahonta, M. J. Kappers, S. J. Haigh, T. J. Pennycook, C. J.
257 Humphreys, R. O. Dusane, and M. A. Moram, *Nano Lett.* **15**, 923 (2015).
- 258 ⁸ Z. Deng, Y. Jiang, W. Wang, L. Cheng, W. Li, W. Lu, H. Jia, W. Liu, J. Zhou, and H. Chen,
259 *Sci. Rep.* **4**, 6734 (2014).
- 260 ⁹ L. Lahourcade, N. C. Coronel, K. T. Delaney, S. K. Shukla, N. A. Spaldin, and H. A. Atwater,
261 *Adv. Mater.* **25**, 2562 (2013).
- 262 ¹⁰ N. Feldberg, J. D. Aldous, P. A. Stampe, R. J. Kennedy, T. D. Veal, and S. M. Durbin, *J.*
263 *Electron. Mater.* **43**, 884 (2014).
- 264 ¹¹ A. Punya and W. R. L. Lambrecht, *Phys. Rev. B* **88**, 075302 (2013).
- 265 ¹² N. Feldberg, B. Keen, J. D. Aldous, D. O. Scanlon, P. A. Stampe, R. J. Kennedy, R. J. Reeves,
266 T. D. Veal, and S. M. Durbin, in *2012 38th IEEE Photovoltaic Specialists Conference* (2012)
267 pp. 2524–2527.
- 268 ¹³ S. Chen, P. Narang, H. A. Atwater, and L.-W. Wang, *Adv. Mater.* **26**, 311 (2014).
- 269 ¹⁴ N. Feldberg, J. D. Aldous, W. M. Linhart, L. J. Phillips, K. Durose, P. a. Stampe, R. J.
270 Kennedy, D. O. Scanlon, G. Vardar, R. L. Field, T. Y. Jen, R. S. Goldman, T. D. Veal, and
271 S. M. Durbin, *Appl. Phys. Lett.* **103**, 042109 (2013).
- 272 ¹⁵ P. C. Quayle, E. W. Blanton, A. Punya, G. T. Junno, K. He, L. Han, H. Zhao, J. Shan, W. R. L.
273 Lambrecht, and K. Kash, *Phys. Rev. B* **91**, 205207 (2015).
- 274 ¹⁶ F. Deng, H. Cao, L. Liang, J. Li, J. Gao, and H. Zhang, *Opt. Lett.* **40**, 1282 (2015).

- 275 ¹⁷ A. N. Fioretti, A. Zakutayev, H. Moutinho, C. Melamed, J. D. Perkins, A. G. Norman, M. Al-
276 Jassim, E. S. Toberer, and A. C. Tamboli, *J. Mater. Chem. C* **3**, 11017 (2015).
- 277 ¹⁸ N. Senabulya, N. Feldberg, R. A. Makin, Y. Yang, G. Shi, C. M. Jones, E. Kioupakis, J. Mathis,
278 R. Clarke, and S. M. Durbin, *AIP Adv.* **6**, 075019 (2016).
- 279 ¹⁹ J. O. McCaldin, T. C. McGill, and C. A. Mead, *Phys. Rev. Lett.* **36**, 56 (1976).
- 280 ²⁰ P. Hohenberg and W. Kohn, *Phys. Rev.* **136**, B864 (1964).
- 281 ²¹ W. Kohn and L. J. Sham, *Phys. Rev.* **140**, A1133 (1965).
- 282 ²² J. Heyd, G. E. Scuseria, and M. Ernzerhof, *J. Chem. Phys.* **118**, 8207 (2003).
- 283 ²³ G. Kresse and J. Hafner, *Phys. Rev. B* **47**, 558 (1993).
- 284 ²⁴ G. Kresse and J. Hafner, *Phys. Rev. B* **49**, 14251 (1994).
- 285 ²⁵ J. P. Perdew, K. Burke, and M. Ernzerhof, *Phys. Rev. Lett.* **77**, 3865 (1996).
- 286 ²⁶ J. Heyd and G. E. Scuseria, *J. Chem. Phys.* **121**, 1187 (2004).
- 287 ²⁷ J. Paier, M. Marsman, K. Hummer, G. Kresse, I. C. Gerber, and J. G. Ángyán, *J. Chem. Phys.*
288 **124**, 154709 (2006).
- 289 ²⁸ R. W. Godby, M. Schlüter, and L. J. Sham, *Phys. Rev. B* **37**, 10159 (1988).
- 290 ²⁹ F. Oba, A. Togo, I. Tanaka, J. Paier, and G. Kresse, *Phys. Rev. B* **77**, 245202 (2008).
- 291 ³⁰ J. L. Lyons, A. Janotti, and C. G. Van de Walle, *Phys. Rev. B* **89**, 035204 (2014).
- 292 ³¹ C. Freysoldt, B. Grabowski, T. Hickel, J. Neugebauer, G. Kresse, A. Janotti, and C. G. Van
293 de Walle, *Rev. Mod. Phys.* **86**, 253 (2014).
- 294 ³² P. E. Blöchl, *Phys. Rev. B* **50**, 17953 (1994).
- 295 ³³ A. Janotti and C. G. Van de Walle, *Phys. Rev. B* **75**, 121201 (2007).
- 296 ³⁴ C. Freysoldt, J. Neugebauer, and C. G. Van de Walle, *Phys. Status Solidi* **248**, 1067 (2011).
- 297 ³⁵ M. Debbichi, T. Sakhraoui, L. Debbichi, and M. Said, *J. Alloys Compd.* **578**, 602 (2013).
- 298 ³⁶ O. Lagerstedt and B. Monemar, *Phys. Rev. B* **19**, 3064 (1979).
- 299 ³⁷ R. R. Reeber, *J. Appl. Phys.* **41**, 5063 (1970).
- 300 ³⁸ P. King, T. Veal, C. Kendrick, L. R. Bailey, S. Durbin, and C. F. McConville, *Phys. Rev. B*
301 **78**, 033308 (2008).
- 302 ³⁹ T. D. Veal, P. D. C. King, S. A. Hatfield, L. R. Bailey, C. F. McConville, B. Martel, J. C.
303 Moreno, E. Frayssinet, F. Semond, and J. Zúñiga-Pérez, *Appl. Phys. Lett.* **93**, 202108 (2008).
- 304 ⁴⁰ J. W. Liu, A. Kobayashi, S. Toyoda, H. Kamada, A. Kikuchi, J. Ohta, H. Fujioka, H. Kumi-
305 gashira, and M. Oshima, *Phys. Status Solidi* **248**, 956 (2011).

- 306 ⁴¹ M. N. Huda, Y. Yan, S.-H. Wei, and M. M. Al-Jassim, *Phys. Rev. B* **78**, 195204 (2008).
- 307 ⁴² A. Janotti and C. G. Van de Walle, *Reports Prog. Phys.* **72**, 126501 (2009).
- 308 ⁴³ A. Janotti and C. G. Van de Walle, *Nat. Mater.* **6**, 44 (2007).
- 309 ⁴⁴ J. L. Lyons, A. Janotti, and C. G. Van de Walle, *J. Appl. Phys.* **115**, 012014 (2014).
- 310 ⁴⁵ J. W. Ager, R. E. Jones, D. M. Yamaguchi, K. M. Yu, W. Walukiewicz, S. X. Li, E. E. Haller,
311 H. Lu, and W. J. Schaff, *Phys. Status Solidi* **244**, 1820 (2007).
- 312 ⁴⁶ J. L. Lyons, A. Janotti, and C. G. Van de Walle, *Appl. Phys. Lett.* **97**, 152108 (2010).
- 313 ⁴⁷ A. N. Fioretti, A. Stokes, M. R. Young, B. Gorman, E. S. Toberer, A. C. Tamboli, and
314 A. Zakutayev, *Adv. Electron. Mater.* **3**, 1600544 (2017).